HHS Public Access

Author manuscript

Bone. Author manuscript; available in PMC 2022 March 01.

Published in final edited form as:

Bone. 2021 March ; 144: 115832. doi:10.1016/j.bone.2020.115832.

The Role of *Zfp467* in Mediating the Pro-osteogenic and Anti-adipogenic Effects on Bone and Bone Marrow Niche

Phuong T. Le[*,a], **Hanghang Liu**[*,a], **Lama Alabdulaaly**[b], **Yosta Vegting**[c], **Isabella L Calle**[a,d], **Francesca Gori**[b], **Beate Lanske**[b], **Roland Baron**[b,e,#], **Clifford J. Rosen**[a,#]

[a]Maine Medical Center Research Institute, Maine Medical Center, Scarborough, ME 04074, USA [b]Division of Bone and Mineral Research, Harvard School of Dental Medicine, Boston, MA 02115, USA [c]University of Amsterdam, Amsterdam UMC, Meibergdreef 9, 1105 AZ, Amsterdam, The Netherlands [d]Graduate Medical Sciences, Boston University School of Medicine, Boston, MA 02118, USA [e]Harvard Medical School, Department of Medicine and Endocrine Unit, Massachusetts General Hospital, Boston, 02115, USA

Abstract

Conditional deletion of the PTH receptor (*Pth1r)* in mesenchymal progenitors reduces osteoblast differentiation and bone mass while enhancing adipogenesis and bone marrow adipose tissue. Mechanistically, PTH suppresses the expression of *Zfp467*, a pro-adipogenic zinc finger transcription factor. Consequently, *Pth1r* deficiency in mesenchymal progenitors leads to increased *Zfp467* expression. Based on these observations, we hypothesized that genetic loss of *Zfp467* would lead to a shift in marrow progenitor cell fate towards osteogenesis and increased bone mass. To test this hypothesis, we generated *Zfp467−/−* mice. *Zfp467−/−* mice (−/−) were significantly smaller than *Zfp467+/+* mice (+/+). μCT showed significantly higher trabecular bone and cortical bone area in −/− vs. +/+, and histomorphometry showed higher structural and dynamic formation parameters in −/− mice vs. +/+. Femoral gene expression including *Alpl, Sp7*, and *Acp5* were increased in −/−mice, whereas *Adiponectin, Cebpa, Lepr*, and *Ppra*γ mRNA were lower in −/−

Corresponding Author: Clifford J Rosen, M.D, Maine Medical Center Research Institute, 81 Research Drive, Scarborough, ME 04074, Tel: (207) 386-8157, Fax: (207) 386-8174, rosenc@mmc.org.

[*]These authors contributed equally to this work.

[#]Co-senior authors

Credit Author Statement

Phuong T. Le: Investigation, Resources, Data Curation, Visualization, Writing - Original Draft
Hanghang Liu: Investigation, Resources, Data Curation, Visualization, Writing - Original Draft
Lama Alabdulaaly: Resources, Data Curation, Visualization, Software, Writing - Original Draft
Yosta Vegting: Resources, Visualization
Isabella L Calle: Resources, Visualization
Francesca Gori: Writing - Review & Editing
Beate Lanske: Data Curation, Software
Roland Baron: Conceptualization, Writing - Review & Editing, Supervision
Clifford J. Rosen: Conceptualization, Writing - Review & Editing, Supervision, Project administration
Clifford J. Rosen takes responsibility for the integrity of the data analysis and is responsible for ensuring that the descriptions are accurate and agreed by all authors

Disclosure Statement: The authors have nothing to disclose.

mice. Similarly, *Fabp4* and *Lep* in the inguinal depot were also decreased in −/− mice. Moreover, marrow adipocyte numbers were reduced in −/− vs +/+ mice ($p<0.007$). *In vitro,* COBs and BMSCs−/− showed more positive ALP and Alizarin Red staining and a decrease in ORO droplets. *Pth1r* mRNA and protein levels were increased in COBs and BMSCs from −/− mice vs +/+ ($p<0.02$ for each parameter, −/− vs. +/+). −/− cells also exhibited enhanced endogenous levels of cAMP vs. control cells. Moreover, in an ovariectomy (OVX) mouse model, *Zfp467*−/− mice had significantly lower fat mass but similar bone mass compared to OVX +/+ mice. In contrast, in a high fat diet (HFD) mouse model, in addition to reduced adipocyte volume and adipogenesis related gene expression in both peripheral and bone marrow fat tissue, greater osteoblast number and higher osteogenesis related gene expression were also observed in −/− HFD mice vs. +/+ HFD mice. Taken together, these results demonstrate that ZFP467 negatively influences skeletal homeostasis and favors adipogenesis. Global deletion of *Zfp467* increases PTHR1, cAMP and bone turnover, hence its repression is a component of PTH signaling and its regulation. These data support a critical role for *Zfp467* in early lineage allocation and provide a novel potential mechanism by which PTH acts in an anabolic manner on the bone remodeling unit.

Graphical Abstract

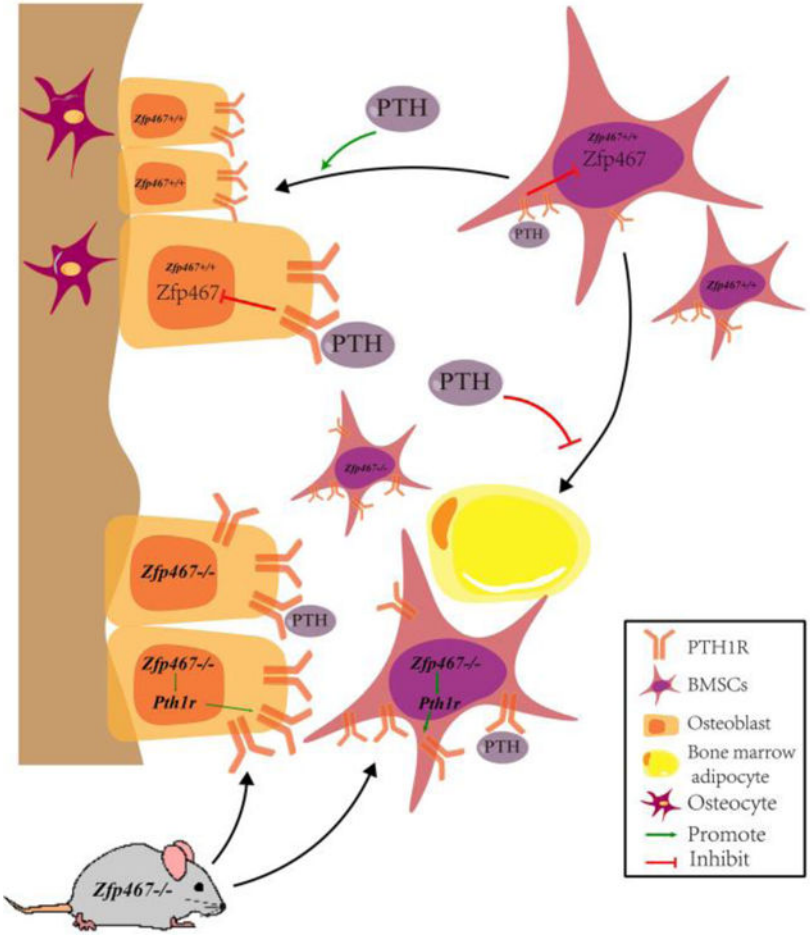

Keywords

Genetic animal models; Bone-fat interactions; PTH; Osteoblasts; Stromal/Stem Cells

Introduction

Zinc finger proteins (ZFPs) are one of the largest classes of transcription factors in eukaryotic genomes.[1] Numerous ZFPs regulate growth and development of normal cells and tissues, including bone, through diverse signal transduction pathways.[2–5] A small but increasing number of ZFPs have been associated with adipogenesis.[6] Quach *et al.* noted that *Zinc finger protein 467* (*Zfp467*) enhanced adipogenesis and was down regulated by PTH in a gene array experiment with a stromal cell line.[7] They also reported that *Zfp467* up regulated *Pparγ,* an essential transcriptional regulator of adipogenesis, and PTH receptor 1 (*Pth1r*). Similar work by You *et al.* noted that *Zfp467* increased *Sost* expression in marrow stromal cells (MSCs) independent of *Pparγ*.[8,9] Finally, we reported that conditional deletion of the *Pth1r* in early mesenchymal progenitors using the *Prx1Cre* led to an increase in *Zfp467* gene expression in marrow adipocytes.[10]

PTH1R is activated by Parathyroid hormone (PTH) and parathydroid hormone-related peptide (PTHrP). Intermittent administration of PTH 1–34, teriparatide, or a PTHrP analog, abaloparatide, stimulates new bone formation through the PTH1R on osteoblasts, leading to lower fracture risk and higher bone mass in postmenopausal women.[11,12] The mechanisms that underlie PTH-driven osteogenesis are multiple, complex and in many cases, redundant. Downstream targets from PTH1R activation include but are not limited to IGF-1, FGF-2, Sclerostin, Wnt signaling, and the BMPs.[13–17] PTH works both on resting osteoblasts, lining cells, and early progenitors in the bone marrow niche.[18,19] Several reports have noted that PTH can drive lineage allocation of mesenchymal skeletal stem cells towards osteogenesis and away from adipogenesis, at least in part through its actions on PKA/cyclic AMP pathway and Wnt signaling pathway.[20–22] Indeed, studies in mice and humans have confirmed that intermittent PTH treatment reduces bone marrow adiposity principally through lineage allocation.[10, 23,24] Recently it has been reported that PTH can directly reduce marrow adipocyte size, due to activation of lipolytic enzymes, and thereby contribute to fatty acid availability in the niche for the working osteoblast.[14,25]

Based on these studies, we hypothesized that *Zfp467*, as a component of PTH signaling, was an essential transcriptional regulator for lineage allocation during osteogenesis and adipogenesis. To test that hypothesis, we took a genetic approach by generating mice with a global deletion of the *Zfp467* gene. Our study demonstrates that *Zfp467* is an important transcription factor that regulates the balance between adipogenesis and osteogenesis in the marrow niche, influencing skeletal homeostasis, and plays an important role in the regulation of PTH1R.

Methods

Mice

Cryopreserved C57BL/6N-Zfp467$^{tm1(KOMP)Vlcg}$ sperms were obtained from UC Davis KOMP Repository (Davis, CA). In order to generate *Zfp467* knockout mice (−/−), *in vitro* fertilization was performed using oocytes obtained from super-ovulated B6.Cg-Edil3$^{Tg(Sox2-cre)1Amc}$/J Sox2Cre female (Jackson Laboratory, Bar Harbor, ME) at the Maine Medical Center Research Institute Transgenic core facility. The resulting −/− founder mice were produced on a mixed C57BL/6J and C57BL/6N background. Mice were bred to produce knockout (−/−) and wild-type littermate control (+/+) mice. Mice were housed in polycarbonate cages on sterilized paper bedding and maintained under 14:10 hour light:dark cycles in the barrier, AAALAC-accredited animal facility at Maine Medical Center Research Institute. All studies were reviewed and approved by the Institutional Animal Care and Use Committee of Maine Medical Center and followed the NIH guidelines for the Care and Use of Laboratory Animals. The experiments herein utilized only females. Males mice are under investigation at this time.

Diet Manipulation

Wild type and −/− mice were randomly assigned to either control (LFD, 10% kcal from fat from Research Diets, Inc., New Brunswick, NJ, USA) or high fat diet (HFD, 60% kcal from fat, Research Diets, Inc.) at 8 weeks of age. Mice were group-housed and fed 3g of HFD per day per mouse with HFD being changed twice a week for a period of 8 weeks, at which time they were sacrificed and tissues were collected for analysis.

Ovariectomy (OVX)

Wild type and −/− mice had access to sterilized water and AIN-93M mature rodent diet (Research Diets, Inc. New Brunswich, NJ) ad libitum. At 8 weeks of age +/+ and −/− were subjected to either OVX or sham operation. Mice were then analyzed 12 weeks after surgery (20 wk of age) before harvesting when serum and tissues were collected for further analysis.

Dual-energy X-ray Absorptiometry (DXA)

Whole body composition exclusive of the head was performed using the PIXImus densitometer (GE-Lunar, Fairfield, CT, USA). The PIXImus was calibrated daily with a phantom provided by the manufacturer.

Micro-computed Tomography (μCT)

Micro-architecture of trabecular bone in the distal tibial metaphysis and cortical bone at the tibial mid-diaphysis were analyzed by a high resolution μCT system (μCT40, Scanco Medical AG, Bruttisellen, Switzerland). Scans were acquired using a 10 μm^3 isotropic voxel size, 70 kVP x-ray tube potential, 114 mA X-ray tube intensity, and 200 ms integration time. Trabecular bone in the distal tibial metaphysis was evaluated in a 1500 μm (150 transverse slices) long region beginning 200 μm superior to the distal growth plate and extending proximally. Trabecular bone in the tibia was segmented from soft-tissue using threshold of 300 mgHA/cm^3. Measurements of trabecular regions included trabecular bone volume

fraction (Tb.BV/TV, %), trabecular number (Tb.N, mm^{-1}), trabecular separation (Tb.Sp, μm), connectivity density (ConnD, $1/mm^3$), and structure model index (SMI). For cortical bone, soft tissue was segmented using a threshold of 696 $mgHA/cm^3$ and then was evaluated in a 500 μm (50 slice) long region at the tibial mid-diaphysis to measure total cross-sectional area (Tt.Ar, mm^2), medullary area (Ma.Ar, mm^2), bone area fraction (Ct.Ar/Tt.Ar, %), cortical tissue mineral density (Ct.TMD, $mgHA/cm^3$), cortical thickness (Ct.Th, mm), and cortical porosity (%). All scans were analyzed using manufacturer software (Scanco, version 4.05). Acquisition and analysis of μCT data were performed in accordance with published guidelines.[26]

Bone Histomorphometry

Mice were intraperitoneally injected with 20 mg/kg calcein and 30 mg/kg alizarin complexones (both were from Sigma, St. Louis, MO) 9 days and 2 days, respectively, prior to sacrifice. Static and dynamic histomorphometry measurements were performed in −/− and +/+ at 16 weeks of age as previously described.[27, 28] Tibiae were analyzed as described and standard nomenclature was used.[29]

Bone Marrow Adipocyte Quantification

Tibiae were harvested and fixed in 10% neutral-buffered formalin (Sigma, St. Louis, MO) immediately after sacrifice for 48 hours before they were transferred to 70% EtOH. Samples were then processed before they were plastic embedded, sectioned, and stained with toluidine blue. Pictures were taken at 20x and stitched together before they were analyzed using BIOQUANT OSTEO software (BIOQUANT, Nashville, TN) to assess marrow adipocytes.

Adipose Tissue Histology

Inguinal fat pads were fixed in 10% neutral-buffered formalin (Sigma, St. Louis, MO) immediately after sacrifice for 48 hours before they were transferred to 70% ethanol. Samples were then paraffin-embedded, sectioned, and stained with hematoxylin and eosin to assess their morphology.

Insulin and Glucose Tolerance Tests (ITT and GTT)

For the insulin tolerance test (ITT), 15 weeks old −/− and +/+ mice were fed ad libitum and i.p injected with insulin at 1U/kg (Sigma, St. Louis, MO). For glucose tolerance test (GTT), 15 weeks old −/− and +/+ mice were fasted overnight before they were i.p injected with 1g/kg of D-(+)-Glucose (Sigma, St. Louis, MO). For both tests, blood was taken from a tail vein and glucose levels were measured using a OneTouch Ultra Glucometer (Lifespan, Inc., Milpitas, CA) at baseline, 15 minutes, 30 minutes, 60 minutes, and 120 minutes post injection.

Calvarial Osteoblast and Bone Marrow Stromal Cell Cultures

Calvaria osteoblasts (COBs) were isolated from calvarias of 3–5-day old +/+ and −/− neonates as previously described.[30,31] Following four digestions using collagenase P (Sigma, St. Louis, MO) and trypsin, cells were then re-suspended in Dulbecco's Modified

Eagle Media (DMEM) with 1% penicillin/streptomycin, 2.5% non-essential amino acids (all were from Life Technologies, Carlsbad, CA), and 10% fetal bovine serum (FBS) (VWR, Radnor, PA). The second passage cells were used for plating and further experiment.

Bone marrow stromal cells (BMSCs) were isolated from tibiae and femurs of 6 weeks old +/+ and −/− mice using previously established protocols.[32] Briefly, tibiae and femurs were cut and spun by centrifuge, cells were then resuspended in complete α-MEM [alpha Minimum Essential Medium (αMEM) with 1% penicillin/streptomycin (Life Technologies, Carlsbad, CA) and 10% FBS (VWR, Radnor, PA)]. The first passage cells were used for plating and further experiment.

Ear Mesenchymal Stem Cells (eMSCs) were isolated from ears of 8 weeks old +/+ and −/− mice as previously described.[33] Briefly, ears from each genotype were removed, chopped, and digested in 2mg/mL collagenase I (Worthington Biochemical Corporation, Lakewood, NJ) for one hour at 37°C. Base Medium [DMEM/F-12 (Life Technologies, Carlsbad, CA), 15% fetal bovine serum (VWR, Radnor, PA), and 100ug/mL primocin (Life Technologies, Carlsbad, CA)] was added to quench collagenase I. Samples were then filtered through a 70um strainer, centrifuged, resuspended and plated in 6-well plate. Medium was changed every other day until cells were 80% confluent before adipocyte differentiation was initiated.

Osteogenic Differentiation and Staining

Osteoblastogenesis of COBs and BMSCs were initiated when cells reached 75–85% confluency using osteogenic induction media [(consisted of complete αMEM, 50μg/mL ascorbic acid, and 8mM beta-glycerophosphate (Sigma, St. Louis, MO)]. Medium was changed every two days. To assess osteoblasts and their mineralization, alkaline phosphatase (ALP) and Alizarin Red staining (ARS) were performed on d7 and d14 after differentiation, respectively. ALP kit was obtained from Sigma (St. Louis, MO) and staining was performed according to the manufacturer's instructions after cell fixation with 10% neutral buffered formalin. For ARS, one percent Alizarin Red solution diluted in dH2O (Sigma; pH 4.2) was used to stain the cells for 30 minutes at room temperature. Cells were then washed a couple of times with water before being visualized under the microscope (Leica DM IRB, TV camera) and taking pictures (ZEISS Efficient Navigation, blue edition).

Adipogenic Differentiation and Oil Red O (ORO) Staining

eMSC and BMSCs were differentiated into adipocytes according to previously published protocol.[32] Briefly, once cells were 100% confluent, adipogenic differentiation was initiated with the addition of adipogenic reagents including 0.5mM IBMX, 1uM Dexamethasone, 10ug/mL insulin, and 1uM Rosiglitazone to the Base Medium [DMEM High Glucose (Life Technologies, Carlsbad, CA), 10% fetal bovine serum (FBS) (VWR, Radnor, PA), 1% penicillin/streptomycin (PS) (Life Technologies, Carlsbad, CA)]. Depends on what day the adipocyte culture was, the adipogenic reagents were added differently in the Base Medium. All adipogenic reagents were purchased from Sigma (St. Louis, MO) except Rosiglitazone was purchased from Cayman Chemical (Ann Arbor, MI). Seven days after adipocyte induction, cells were fixed with 10% neutral buffered formalin and were ready for ORO staining.

For ORO staining, fixed cells were washed with 60% isopropanol (Sigma, St. Louis, MO) before stained with ORO working solution (3.5mg/mL ORO stock solution 3:2 diluted in water) (Sigma, St. Louis, MO) for 15 minutes. Cells were then washed a couple of times with water before being visualized under the microscope (Leica DM IRB, TV camera) and taking pictures (ZEISS Efficient Navigation, blue edition).

RNA Isolation and Real-time PCR

Total RNA was isolated using a standard TRIzol extraction method for femurs. Briefly, whole femur was crushed and homogenized in 1mL of TRIZOL (Life Technologies, Carlsbad, CA) before 200uL of Chloroform (Sigma, St. Lois, MO) was added prior to centrifugation at 11,000rpm for 15 minutes at 4°C. Aqueous phase was then removed and transferred to a new tube, isopropanol was added before the centrifugation step was repeated to collect the pellet. This pellet was washed 3 times with 75% ethanol. At the last wash, supernatant was discarded, and the pellet was air dried before it was resuspended in DEPC water. The resuspended RNA was then quantified and assessed for its quality using the Nanodrop 2000 Spectrophotometer (Life Technologies, Carlsbad, CA). cDNA was generated using the High Capacity cDNA Reverse Transcription kit (Life Technologies, Carlsbad, CA) according to the manufacturer's instructions. Quantification of mRNA expression was carried out using an AzuraQuant™ Green Fast qPCR Mix LoRox (Azura Genomics, Raynham, MA) and an iQ™5 multicolor Real-Time PCR detection system (BioRad, Hercules, CA). *Hprt* was used as internal standard control gene. Primers were purchased from Primer Design (Eastleigh, United Kingdom) and Integrated DNA Technologies (IDT, Coralville, IA) (Supplemental Table 1).

Western Blot

Proteins for undifferentiated COBs and BMSCs cells were extracted by scraping the culture wells in the presence of protein lysis buffer composed of 0.5 M Tris-HCl (pH 6.8), 4 M glycerol, and 10% sodium dodecyl sulfate (BioRad, Hercules, CA). Proteins were subjected to Mini-Protean TGX Precast Gels (BioRad, Hercules, CA) before being transferred onto a polyvinyldene fluoride membrane (BioRad, Hercules, CA). The membranes were blocked in 5% nonfat dry milk for 1h and then incubated in primary antibody overnight at 4ºC. Horseradish peroxidase conjugated secondary antibody and chemiluminescence reagent were used to detect the proteins. Antibodies are listed in Supplemental Table 2.

cAMP ELISA Assay

Intracellular cAMP levels in COBs and BMSCs were detected using the Mouse/Rat cAMP Assay Parameter™ Kit (R&D Systems, Minneapolis, MN) according to the manufacturer's instructions. The assay sensitivity was 0.79pmol/mL. The intra-assay and inter-assay variations were 3.6% and 7.3%, respectively. All measurements were performed in duplicate. Furthermore, protein quantity was estimated using the Pierce® BCA Protein Assay Kit (Life Technologies, Carlsbad, CA) according to the manufacturer's guidelines for ELISA normalization.

Statistical Analyses

All data are expressed as the mean ± standard deviation of the mean (SD) unless otherwise noted. Results were analyzed for statistically differences using Student's *t*-test or 2-way ANOVA followed by Bonferroni's multiple comparison *post hoc* test where appropriate. All statistics were performed with Prism 6 statistical software (GraphPad Software, Inc., La Jolla, CA). A *p*-value of less than 0.05 was considered statistically significant.

Results

Zfp467−/− mice are smaller and have less body fat vs. littermate controls

We initially sought to determine the whole body phenotype of the globally deficient *Zfp467* −/− mice. We found that *Zfp467−/−* mice are 7.6% (p=0.0176) and 12.7% (p=0.0006) smaller compared to +/+ mice at 8 and 16 weeks, respectively. This difference could be accounted for by their 16.2% (p=0.0172) and 34.4% (p=0.0002) reduction in total fat and their 5.8% (p=0.0514) and 6.0% (p=0.0300) reduction in lean mass at 8 and 16 weeks, respectively (Fig. 1A). Both total and femoral aBMD and aBMC were significantly lower in −/− at 8 weeks (p=0.0002 and p=0.005) but by 16 weeks, total aBMC (p=0.730) and femoral BMD (p=0.847) and BMC (p=0.873) in −/− were similar to the +/+ mice (Fig. 1A).

Zfp467−/− mice have higher trabecular and cortical bone mass than controls

μCT was performed and analyzed on 16 weeks old +/+ and −/− tibial metaphysis and cortical bone at the tibial mid-diaphysis. *Zfp467−/−* had 41% higher trabecular bone volume fraction (Tb.BV/TV, p=0.0023), 35% higher trabecular bone mineral density (Tb.BMD, p=0.0012), 79% greater connectivity density (Conn.D, p=0.0010), and 21% higher trabecular number (Tb.N, p=0.0002) with a significant 17% and 11% decrease in trabecular separation (Tb.Sp, p=0.0002) and structural model index (SMI, p=0.0051), respectively (Fig. 1B).

In addition, total area (Tt. Ar) was significantly lower in −/− cortical bone compared to +/+ (p = 0.0060); however, cortical area/total area (Ct.Ar/Tt.Ar) and cortical thickness (Ct.Th) were significantly higher in the −/− mice (p=0.0287 and p=0.0560). Conversely, marrow area (Ma.Ar) and cortical porosity (Ct. Porosity) were significantly lower in −/− compared to +/+ mice (p=0.0042 and p=0.0030) with no difference observed in cortical tissue mineral density (Ct.TMD) (p=0.2767) (Fig. 1B).

Increased trabecular bone mass in *Zfp467−/−* is associated with increased bone formation and turnover

To assess the cellular activities that contributed to increased bone mass in −/− mice, we performed static and dynamic histomorphometry on the proximal tibia at 16 weeks of age. Consistent with μCT, histomorphometric analysis showed that bone volume/tissue volume (BV/TV, p=0.0018), trabecular thickness (Tb.Th, p=0.0175), and trabecular number (Tb.N, p=0.0105) were markedly increased while trabecular separation (Tb.Sp, p=0.0224) was significantly decreased in −/− compared to +/+ mice. Additionally, mineral surface/bone surface (MS/BS, p=0.0053), mineral apposition rate (MAR, p=0.0034), and bone formation rate/bone surface (BFR/BS, p=0.0007) were also markedly increased in −/− compared to +/+

mice. However, the osteoblasts surface/bone surface (Ob.S/BS, p=0.8458) and the number of osteoblast/bone perimeter (N.Ob/B.Pm, p=0.9571) were not different between genotypes, suggesting primarily increased osteoblast activity. Interestingly, osteoclast surface/bone surface (Oc.S/BS, p=0.0437) was also significantly, albeit modestly, elevated in −/− with a trend toward an increase in number of osteoclasts/bone perimeter (N.Oc/B.Pm, p=0.1356) (Fig. 2A).

In addition to μCT and histomorphometry, qRT-PCR was performed in whole femurs of 16 weeks old +/+ and −/− mice. Not surprisingly, markers of osteoblast differentiation including *Alp* (p=0.0168) and *Sp7* (p=0.0043) as well as a marker of osteoclast activity *Acp5* (p=0.0183) were significantly increased in −/− mice. Most interestingly, *Pthr1* expression was 35% higher in −/− compared to +/+ (p=0.0004). No difference was found among *Runx2, Col1, Ocn, Opg and Rankl* (data not shown). To elucidate possible mechanisms responsible for the increase in bone mass observed in −/− mice, and since *Zfp467* can increase *Sost* expression,[25] we also looked at downstream Wnt signaling markers such as *Sost* (p=0.1655), *Axin-2* (p=0.6334), *Lef-1* (p=0.0800), *and Dkk-2* (p=0.2682). However, no changes were observed in those gene markers (Fig. 2B).

Zfp467−/− have reduced peripheral and marrow adipose tissue

Although we did not observe any differences in inguinal, gonadal, and brown adipose tissue weights between +/+ and −/− mice (data not shown), histology H&E staining of the inguinal and gonadal fat pads showed markedly smaller adipocyte sizes in −/− mice. Similarly, adipocyte gene expression markers in 16 weeks old inguinal fat pads also showed a significant decrease in *Lep* (p=0.0479) and *Fabp4* (p=0.0491) in −/− compared to +/+, although no difference was found for *Adiponectin* and *Cebp-α* (data not shown). Moreover, *Ucp-1* was down-regulated in −/− inguinal fat tissues (p=0.006), but other genes related to development of brown adipocytes such as *Cidea* (p=0.0878), *DiO2* (p=0.5327), *Pgc1a* (p=0.7360), *and Prdm16* (p=0.3436) showed no difference between genotypes (Fig. 3A).

To quantitate bone marrow adipocyte tissue (BMAT), we used BIOQUANT OSTEO software to analyze images stained with toluidine blue from tibiae of 16 weeks old +/+ and −/−. There was a 67% reduction in marrow adipocyte numbers in −/− compared to +/+ (p=0.0074). Additionally, −/− adipocyte volume (p=0.0010) and adipocyte volume/tissue volume (Ad.V/TV, p=0.0023) were also significantly reduced. On the other hand, and in contrast with other fat depots, there was no difference observed in adipocyte size between genotypes (p=0.8924) in BMAT. Furthermore, gene expression levels of *Adiponectin* (p=0.0114), *Cebpa* (p=0.0267), *Lepr* (p=0.0003), and *Pparγ* (p=0.0002) in whole femur were significantly lower in −/− mice vs. +/+ (Fig. 3B).

Zfp467−/− mice have improved glucose tolerance but no differences in insulin tolerance vs. controls

Because *Zfp467*−/− have a significant lower total fat mass, lower lean mass, smaller peripheral adipocyte sizes, and less marrow adipocytes, we wanted to determine if −/− have an enhanced glucose clearance and increased insulin sensitivity; therefore, we examined glucose clearance rate using ITT and GTT. Blood glucose levels in −/− mice were

significantly lower in the glucose tolerance test (GTT) compared to +/+ (p=0.0030 for 15 min, and p=0.0003 for 30 min after test). However, in an insulin tolerance test, −/− mice showed similar blood glucose changes as +/+ mice, both at baseline and other time points after insulin injection (Fig. 4). The GTT and ITT results are consistent with the reduced total fat mass noted in the *Zfp467−/−* mice.

Zfp467−/− showed increased osteogenesis and decreased adipogenesis *in vitro*

Cultures from both COBs and BMSCs of −/− mice showed an increase in the amount of Alkaline Phosphatase (ALP) staining in addition to an increase in matrix mineralization visualized by Alizarin Red staining (ARS) (Fig. 5A, B). It has been previously shown that COBs in osteogenic media have progenitors that can differentiate into adipocytes with lipid dropletsl highlighted by ORO.[34] Interestingly, −/− COBs exhibited less ORO staining compared to +/+ (Fig. 5A). Additionally, *in vitro* eMSC adipogenesis cultures revealed a significant decrease in lipid droplets stained with ORO in −/− compared to +/+ (Supplemental Figure 1A). However, *in vitro* BMSC adipogenic cultures did not reveal a significant decrease in lipid droplets stained with ORO in −/− vs. +/+ (Fig. 5B).

Not surprisingly, markers of osteoblast differentiation including *Alp* and *Sp7* were significantly up-regulated in −/− COBs (p=0.037 and p=0.0195) and BMSCs (p=0.0012 and p=0.0035) after 7 days of differentiation. Furthermore, expression level of *Rankl* (p=0.0255) was also higher in −/− COB cells. Consistent with the ORO stained data, reduced gene expression levels of adipogenic related genes such as *Adiponectin* was only observed in −/− COBs (p=0.0058) but not in BMSCs (p=0.3016). However, no difference was observed in other adipogenic genes such as *Cebp-α* and *Ppar-γ* both in COBs (p=0.4679 and p=0.9481) and BMSCs (p=0.5331 and p=0.2861) (Fig. 5A, B).

To determine if there was a difference in colony forming units between +/+ and −/−, crystal violet staining was performed in BMSCs. No differences in staining of BMSCs were observed prior to differentiation. (Supplemental Figure 1B).

Zfp467−/− have greater *Pth1r* expression level and higher intracellular cAMP level

Consistent with the *in vivo* data, higher expression levels of *Pth1r* were observed in both −/− COBs (p=0.0032 for qPCR and p=0.0082 for western blot) and BMSCs (p=0.0014 for qPCR and p=0.0236 for western blot) (Fig. 5C, D). Additionally, baseline cAMP ELISA level in COBs −/− cells displayed a 3-fold higher level compared to +/+ (p=0.0003) while cAMP level in BMSCs showed no difference at baseline (Fig. 5E).

Zfp467−/− were resistant to OVX induced adiposity but not bone loss

Based on the above data that ZFP467 may have a pro-adipogenic and anti-ostegenic effect on bone and bone marrow niche, we established OVX mice model to see whether *Zfp467 −/−* could protect bone from OVX induced bone loss.

After OVX, increased fat mass (p=0.0004 and p=0.0378) and decreased aBMD (p=0.0095 and p=0.0002), fBMC (p=0.0019 and p=0.0014) were found in both *Zfp467+/+* and *Zfp467−/−* mice, while decreased aBMC and fBMD were only observed in *Zfp467−/−* mice

compared to sham surgery group. OVX *Zfp467+/+* mice showed significantly higher inguinal fat weight (p=0.0043) and gonadal fat weight (p=0.0158) compared to sham *Zfp467+/+* mice (Fig. 6A). Interestingly, no difference was found in *Zfp467−/−* mice between OVX and sham group for inguinal and gonadal fat weight, and OVX *Zfp467−/−* mice had lower inguinal fat weight than OVX *Zfp467+/+* mice (p=0.0256) (Fig. 6A). We did not find differences in body weight, fat free mass, and BAT weight between either genotypes or with OVX (Fig. 6A)

uCT revealed that both *Zfp467+/+* mice and *Zfp467−/−* mice had significantly lower Tb. BV/TV (p<0.0001 and p<0.0001), Tb.N (p<0.0001 and p<0.0001), Ct.Ar (p=0.0054 and p=0.0003) and higher Tb.Sp (p<0.0001 and p<0.0001) with OVX compared to sham surgery group, respectively. OVX *Zfp467−/−* mice also showed decreased Conn.D (p=0.0021) relative to the sham group. No difference was found in Tb.Th, Tt.Ar, Ma.Ar, Ct.TMD and Cont.Porosity between either genotypes or OVX treatment (Fig. 6B).

Zfp467−/− were resistant to high fat diet-induced adiposity and weight gain

Since *Zfp467 −/−* mice showed significant decreases in both peripheral and bone marrow fat, *Zfp467* could also be a promising target to rescue high fat diet induced fat accumulation and bone loss.

On a high fat diet (HFD), +/+ mice had significantly increased body weight (p=0.0026) due to both higher fat mass (p=0.0027) and fat free mass (p=0.0197) compared to a LFD (Figure 5A). Additionally, +/+ mice on a HFD showed greater inguinal and gonadal fat weight compared to both low fat diet (LFD) +/+ mice (p=0.0075 and 0.0017, respectively). −/− mice on a HFD were resistant to weight gain and total fat mass increase, compared to a LFD (p=NS); hence, there was a strong genotype effect of HFD (p=0.03 and 0.008, respectively −/− vs +/+). Although −/− mice showed slightly decreased in aBMD with HFD compared to LFD (p=0.03) and +/+ HFD (p=0.03) mice, no differences were found in aBMC, fBMD and fBMC between either genotypes or diet treatment (Fig. 7A).

Zfp467−/− had greater osteoblast numbers with HFD vs. *Zfp467+/+*

On a HFD, *Zfp467−/−* mice by uCT showed higher Tb.N (p=0.0050), lower Tb.Sp (p=0.0065) but lower Tb.Th (p=0.0030) compared to *Zfp467+/+* mice (Fig. 7B, C). No differences were found for Tb.BV/TV, Conn.D, SMI, Ct.Ar, Tt.Ar, Ma.Ar, Ct. Th, Ct.TMD and Ct. Porosity between either genotypes or diet treatment (Fig. 8B, C). Histomorphometry suggested similar results; there were no differences in BV/TV, Tb.N, Tb.Th, Tb.Sp, MS/BS, MAR and BFR/BS between either genotypes or diet treatment. However, significantly higher Ob.S/BS and N.Ob/B.Pm were found in −/− mice on a HFD compared to +/+ mice (p=0.0325 and 0.0499, respectively) on a HFD and LFD −/− mice (p=0.0055 and 0.0063, respectively). Oc.S/BS and N.Oc/B.Pm showed no differences between either genotypes or diet treatment (Fig. 8A).

Whole femur qPCR data further confirmed that higher gene expression level of *Pth1r* (p=0.0422), *Sp7* (p=0.0303), *Runx2* (p=0.0546), *Ocn* (p=0.0187) as well as *Ctsk* (p=0.0357) were observed in −/− mice on a HFD compared to HFD +/+ mice. No difference was found in *Acp5* and *Rankl* (Fig. 8B).

Peripheral and marrow fat was less in *Zfp467−/−* mice on HFD vs. *Zfp467+/+*

With HFD, *Zfp467+/+* mice showed increased adipocyte size and gene expression of *Leptin* (p=0.0035) but lower gene expression of *Cebpb* (p=0.0198) in inguinal fat pad compared to LFD. Gene expression of *Leptin* in HFD *Zfp467−/−* mice was significantly lower than HFD *Zfp467+/+* mice (p=0.0235), but expression of *Cebpb* in HFD *Zfp467−/−* mice was higher than HFD *Zfp467+/+* mice (p=0.0366) (Fig. 9A). We did not find any differences for gene expression of *Adiponectin, Leptin receptor, Fabp4* and *Pparg* in bone marrow between either genotypes or diet treatment. HFD *Zfp467+/+* mice showed significantly increased adipocyte number (p=0.0029), Ad.V (p<0.0001), Ad.V/TV (p=0.0001) and increased adipocyte size (p=0.0544) compared to LFD *Zfp467+/+* mice. But, no difference was found in *Zfp467−/−* mice between LFD and HFD for marrow adipocyte number, and HFD *Zfp467−/−* mice had remarkably lower Ad.V (p<0.0001) and Ad.V/TV (p=0.0008) compared to HFD *Zfp467+/+* mice (Fig. 9B).

Discussion

In the current work, we demonstrate the importance of the zinc finger protein ZFP467 for both lineage allocation and cellular activity in progenitors of the osteoblast lineage. *Zfp467* was originally isolated from mouse hematogenic endothelial LO cells as an OSM-inducible mRNA;[35] its encoding protein ZFP467 belongs to the Kruppel like family of transcription factors. While *Zfp467* is expressed ubiquitously, it was reported to be an important mediator of BMSC differentiation into the adipogenic or osteogenic lineage.[7] Using a genetic strategy, we show that the global absence of *Zfp467* resulted in a significant increase in trabecular bone volume, accompanied by a marked reduction in peripheral and marrow adipose tissue and improved glucose tolerance. Consistent with the *in vivo* phenotype, we report that most of the major adipogenic differentiation factors were also reduced in the marrow and peripheral fat tissue of the null mice, while skeletal genes were up regulated. Importantly, whole femur, bone marrow stromal cells, and calvarial osteoblast gene expression had a ~40% increase in *Pth1r* expression in the −/− mice compared to littermate controls. These data are consistent with our previous work that showed deletion of the *Pth1r* in bone marrow mesenchymal progenitors resulted in low bone mass, high bone marrow adiposity, increased bone resorption, and loss of PTH-induced suppression of *Zfp467* expression in cortical bone.[10] Hence loss of *Zfp467* can result in promotion of bone formation accompanied by a reduction in bone marrow adipocytes and greater differentiation of osteoblasts.

In our *a priori* hypothesis we suspected there was constitutive up regulation of *Pth1r* in osteoblasts, a potential marker of greater bone formation. This was confirmed in both calvarial osteoblasts and bone marrow stromal cells undergoing osteogenic differentiation *in vitro*. In addition, PTH1R protein levels were also enhanced in COBs and BMSCs −/− cells. Furthermore, we found both COBs and BMSCs from −/− mice showed greater differentiation into osteoblasts in osteogenic media but less differentiation into adipocytes compared to controls. Additionally, −/− cells also showed higher cAMP level at baseline. Taken together, higher rates of osteogenesis, enhanced *Rankl* expression, and decreased

adipogenesis in −/− cells are likely related to greater signaling from the PTH1R, possibly due to its higher expression level.

Previously, *Zfp467* was found to bind to and regulate the expression of *Sost* and impair bone formation through the modulation of Wnt signaling.[9,36] However, we found no differences in *Sost* and Wnt pathway genes including *Lef-1*, *Axin2,* and *Dkk-2* between genotypes in either whole bone (Fig. 2B) or *in vitro* cell culture (data not shown). Similarly, another potential downstream target of *Zfp467*, *Ppar-γ*, showed no differences in expression between genotypes (data not shown).

Based on the pro-adipogenic and anti-osteogenic role of *Zfp467* in female mice, we established an OVX model to determine whether *Zfp467 −/−* could rescue OVX induced bone loss. Although we observed significantly decreased fat weight in *Zfp467 −/−* mice compared to +/+ mice after OVX, no remarkable differences were found regarding trabecular bone volume, number, thickness, and cortical bone area between genotypes after OVX. In contrast, more trabeculae and greater number of osteoblasts were found in HFD *Zfp467 −/−* mice than HFD *Zfp467 +/+* mice. Not surprisingly, *Zfp467 −/−* female mice with HFD also showed remarkably lower body weight and fat mass than *Zfp467 +/+* female mice, and no differences were found between diet treatment in *Zfp467 −/−* mice regarding body composition. Similarly, significantly decreased bone marrow fat and adipogenesis related gene expression were also observed in HFD *Zfp467 −/−* mice compared to HFD *Zfp467 +/+* female mice. These data suggested that *Zfp467 −/−* showed great resistance to OVX and HFD induced fat accumulation but cannot rescue OVX induced bone loss.

PTH can induce lipolysis in adipose tissue via PKA signaling;[14] this is consistent with our finding that the adipose phenotype of the *Zfp467−/−* mice was reduced, lending credence to the likelihood that PTH may mediate not only lineage allocation but also whole body composition changes. However, our model was a global deletion, and therefore conclusions about changes in fat mass will await conditional deletion using the *Adipo Cre* mouse, which is currently underway. This may also provide insights into the role of PTH induced lipolysis. In that vein, we recently showed that PTH could enhance lipolysis from marrow adipocytes *in vitro*, leading to the possibility that those fatty acids could be a source of energy for differentiating osteoblasts.[24] *Zfp467−/−* mice have lower marrow adipose volume coincident with higher bone mass and bone formation, with or without HFD, consistent with previous reports that PTH administration can reduce adipocyte volume in the marrow.[10] However, interestingly enough, individual marrow adipocyte size was not different by genotype with or without HFD. Notwithstanding, the difficulty in isolating marrow adipocytes and determining lipolytic activity *ex vivo* limit our conclusions about the role of PTH in regulating marrow adiposity and subsequently bone remodeling. On the other hand, it is interesting to speculate on the effects of PTH on whole body homeostasis, particularly since the *Zfp467−/−* had less body fat, and markedly smaller peripheral adipocytes, but no indication of ‘beiging’ or browning of adipose depots. Importantly despite these changes, body composition in postmenopausal women receiving intermittent PTH has not shown a clear effect on body weight or adipose distribution. Further studies will be needed to understand how PTH may mediate lipolysis and body composition both in marrow and peripheral fat.

In conclusion, our data suggest a critical role for *Zfp467* in the reciprocal adipogenic and osteogenic cell fate decision in bone and the bone marrow niche. Our studies also support the inverse association between levels of PTH1R and *Zfp467* as reported previously by Quach et al[7]. As such, *Zfp467* can be added to the growing list of downstream effectors of PTH that mediate its actions on osteoblasts and adipocytes, although the precise mechanism of the putative suppression of Zfp467 by PTH requires further studies.

Supplementary Material

Refer to Web version on PubMed Central for supplementary material.

Acknowledgements

Study design: Clifford J. Rosen and Roland Baron. Study conduct: Phuong T. Le and Hanghang Liu. Data collection: Phuong T. Le, Hanghang Liu, Yosta Vegting and Isabella L Calle. Data analysis: Phuong T. Le, Hanghang Liu and Lama Alabdulaaly. Data interpretation: Phuong T. Le, Hanghang Liu, Roland Baron and Clifford J. Rosen. Consulting on experiments: Beate Lanske. Drafting manuscript: Phuong T. Le and Hanghang Liu. Revising manuscript content: Francesca Gori, Roland Baron and Clifford J. Rosen. Approving final version of manuscript: Roland Baron and Clifford J. Rosen. Clifford J. Rosen takes responsibility for the integrity of the data analysis. The research reported in this publication was supported by NIH grant R01 DK112374 to Roland Baron and Cliff Rosen. This work utilized services of the Maine Medical Center Research Institute (MMCRI) Molecular Phenotyping Core, which is supported by NIH/NIGMS P30GM106391, the Histopathology and Histomorphometry Core, which is supported by NIH/NIGMS P30GM106391, P20GM121301, and P30103392, and the Mouse Transgenic and In Vivo Imaging Core which is supported by NIH/NIGMS P30GM103392. The content is solely the responsibility of the authors and does not necessarily represent the official views of the National Institutes of Health. The authors thank Terry Henderson and Dorothy Hu for technical assistance. Dr. Lanske current address is: Radius Health Inc., Waltham, MA 02451, USA

Reference

1. JM B. Zinc fingers and other metal-binding domains. Elements for interactions between macromolecules. J Biol Chem. 1990;29:31.
2. Ganss B JA. Zinc finger transcription factors in skeletal development. Crit Rev Oral Biol Med. 2004;15:282–97. [PubMed: 15470266]
3. Leon O RM. Zinc fingers: DNA binding and protein-protein interactions. Biol Res. 2000;33:21–30. [PubMed: 11021307]
4. Addison WN, Fu MM, Yang HX, Lin Z, Nagano K, Gori F, et al. Direct transcriptional repression of Zfp423 by Zfp521 mediates a bone morphogenic protein-dependent osteoblast versus adipocyte lineage commitment switch. Mol Cell Biol. 8 2014;34(16):3076–85. [PubMed: 24891617]
5. Kiviranta R, Yamana K, Saito H, Ho DK, Laine J, Tarkkonen K, et al. Coordinated transcriptional regulation of bone homeostasis by Ebf1 and Zfp521 in both mesenchymal and hematopoietic lineages. J Exp Med. 5 6 2013;210(5):969–85. [PubMed: 23569325]
6. Wei S, Zhang L, Zhou X, Du M, Jiang Z, Hausman GJ, et al. Emerging roles of zinc finger proteins in regulating adipogenesis. Cell Mol Life Sci. 12 2013;70(23):4569–84. [PubMed: 23760207]
7. Quach JM, Walker EC, Allan E, Solano M, Yokoyama A, Kato S, et al. Zinc finger protein 467 is a novel regulator of osteoblast and adipocyte commitment. J Biol Chem. 2 11 2011;286(6):4186–98. [PubMed: 21123171]
8. You L, Pan L, Chen L, Chen JY, Zhang X, Lv Z, et al. Suppression of zinc finger protein 467 alleviates osteoporosis through promoting differentiation of adipose derived stem cells to osteoblasts. J Transl Med. Jan 17 2012;10:11.
9. You L, Chen L, Pan L, Gu WS, Chen JY. Zinc finger protein 467 regulates Wnt signaling by modulating the expression of sclerostin in adipose derived stem cells. Biochem Biophys
10. Fan Y, Hanai JI, Le PT, Bi R, Maridas D, DeMambro V, et al. Parathyroid Hormone Directs Bone Marrow Mesenchymal Cell Fate. Cell Metab. 3 7 2017;25(3):661–72. [PubMed: 28162969]

11. Jilka RL, Weinstein RS, Bellido T, Roberson P, Parfitt AM, & Manolagas SC. Increased bone formation by prevention of osteoblast apoptosis with parathyroid hormone. J Clin Invest. 1999;104(4):439–46. [PubMed: 10449436]
12. Kim SW, Pajevic PD, Selig M, Barry KJ, Yang JY, Shin CS, et al. Intermittent parathyroid hormone administration converts quiescent lining cells to active osteoblasts. J Bone Miner Res. 10 2012;27(10):2075–84. [PubMed: 22623172]
13. Li X, Qin L, Bergenstock M, Bevelock LM, Novack DV, Partridge NC. Parathyroid hormone stimulates osteoblastic expression of MCP-1 to recruit and increase the fusion of pre/osteoclasts. J Biol Chem. 11 9 2007;282(45):33098–106. [PubMed: 17690108]
14. Mansoori MN, Shukla P, Singh D. Combination of PTH (1–34) with anti-IL17 prevents bone loss by inhibiting IL-17/N-cadherin mediated disruption of PTHR1/LRP-6 interaction. Bone. 12 2017;105:226–36. [PubMed: 28935557]
15. Esen E, Lee SY, Wice BM, Long F. PTH Promotes Bone Anabolism by Stimulating Aerobic Glycolysis via IGF Signaling. J Bone Miner Res. 11 2015;30(11):1959–68. [PubMed: 25990470]
16. Wojda SJ, Donahue SW. Parathyroid hormone for bone regeneration. J Orthop Res. 10 2018;36(10):2586–94. [PubMed: 29926970]
17. Yu B, Zhao X, Yang C, Crane J, Xian L, Lu W, et al. Parathyroid hormone induces differentiation of mesenchymal stromal/stem cells by enhancing bone morphogenetic protein signaling. J Bone Miner Res. 9 2012;27(9):2001–14. [PubMed: 22589223]
18. Bellido T, Ali AA, Plotkin LI, Fu Q, Gubrij I, Roberson PK, et al. Proteasomal degradation of Runx2 shortens parathyroid hormone-induced anti-apoptotic signaling in osteoblasts. A putative explanation for why intermittent administration is needed for bone anabolism. J Biol Chem. 12 12 2003;278(50):50259–72. [PubMed: 14523023]
19. Goltzman D. Physiology of Parathyroid Hormone. Endocrinol Metab Clin North Am. 12 2018;47(4):743–58. [PubMed: 30390810]
20. Li C, Xing Q, Yu B, Xie H, Wang W, Shi C, et al. Disruption of LRP6 in osteoblasts blunts the bone anabolic activity of PTH. J Bone Miner Res. 10 2013;28(10):2094–108. [PubMed: 23609180]
21. Crowell JA CC, Toverud SU, & Boass A. Effects of Vitamin D and Parathyroid Hormone on Cyclic AMP Production by Bone Cells Isolated from Rat Calvariae. Calcif Tissue Int 1984;36(2):320–6. [PubMed: 6088011]
22. Ozkurt IC, Pirih FQ, Tetradis S. Parathyroid hormone induces E4bp4 messenger ribonucleic acid expression primarily through cyclic adenosine 3',5'-monophosphate signaling in osteoblasts. Endocrinology. 8 2004;145(8):3696–703. [PubMed: 15087429]
23. Calvi LM, Sims NA, Hunzelman JL, Knight MC, Giovannetti A, Saxton JM, et al. Activated parathyroid hormone/parathyroid hormone–related protein receptor in osteoblastic cells differentially affects cortical and trabecular bon. J Clin Invest. 2001;107(3):277–86. [PubMed: 11160151]
24. Maridas DE, Rendina-Ruedy E, Helderman RC, DeMambro VE, Brooks D, Guntur AR, et al. Progenitor recruitment and adipogenic lipolysis contribute to the anabolic actions of parathyroid hormone on the skeleton. FASEB J. Feb 2019;33(2):2885–98.
25. Sara Larsson HAJ, Olga Göransson, Eva Degerman, Cecilia Holm. Parathyroid hormone induces adipocyte lipolysis via PKA-mediated phosphorylation of hormone-sensitive lipase. Cellural Signaling. 2016;28:204–13.
26. Bouxsein ML, Boyd SK, Christiansen BA, Guldberg RE, Jepsen KJ, Muller R. Guidelines for assessment of bone microstructure in rodents using micro-computed tomography. J Bone Miner Res. 7 2010;25(7):1468–86. [PubMed: 20533309]
27. Rydziel S, Stadmeyer L, Zanotti S, Durant D, Smerdel-Ramoya A, Canalis E. Nephroblastoma overexpressed (Nov) inhibits osteoblastogenesis and causes osteopenia. J Biol Chem. 7 6 2007;282(27):19762–72. [PubMed: 17500060]
28. Beamer WG, Shultz KL, Ackert-Bicknell CL, Horton LG, Delahunty KM, Coombs HF 3rd, et al. Genetic dissection of mouse distal chromosome 1 reveals three linked BMD QTLs with sex-dependent regulation of bone phenotypes. J Bone Miner Res. 8 2007;22(8):1187–96. [PubMed: 17451375]

29. Dempster DW, Compston JE, Drezner MK, Glorieux FH, Kanis JA, Malluche H, et al. Standardized nomenclature, symbols, and units for bone histomorphometry: a 2012 update of the report of the ASBMR Histomorphometry Nomenclature Committee. J Bone Miner Res. 1 2013;28(1):2–17. [PubMed: 23197339]

30. Rosen CJ, Dimai HP, Vereault D, Donahue LR, Beamer WG, Farley J, Linkhart S, Linkhart T, Mohan S, & Baylink D. Circulating and skeletal insulin-like growth factor-I (IGF-i) concentrations in two inbred strains of mice with different bone mineral densities. Bone. 1997;21(3):217–23. [PubMed: 9276086]

31. Kawai M, Breggia AC, DeMambro VE, Shen X, Canalis E, Bouxsein ML, et al. The heparin-binding domain of IGFBP-2 has insulin-like growth factor binding-independent biologic activity in the growing skeleton. J Biol Chem. 4 22 2011;286(16):14670–80. [PubMed: 21372140]

32. Maridas DE, Rendina-Ruedy E, Le PT, Rosen CJ. Isolation, Culture, and Differentiation of Bone Marrow Stromal Cells and Osteoclast Progenitors from Mice. J Vis Exp. 1 6 2018(131).

33. Liaw L, Prudovsky I, Koza RA, Anunciado-Koza RV, Siviski ME, Lindner V, et al. Lipid Profiling of In Vitro Cell Models of Adipogenic Differentiation: Relationships With Mouse Adipose Tissues. J Cell Biochem. 9 2016;117(9):2182–93. [PubMed: 26910604]

34. Bellows CG, Wang YH, Heersche JN, & Aubin JE. 1,25-dihydroxyvitamin D3 stimulates adipocyte differentiation in cultures of fetal rat calvaria cells: comparison with the effects of dexamethasone. Endocrinology. 1994;134(5):2221–9. [PubMed: 8156925]

35. Nakayama K, Kim K-W, & Miyajima A. A novel nuclear zinc finger protein EZI enhances nuclear retention and transactivation of STAT3. The EMBO Journal. 2002;21:6174–84. [PubMed: 12426389]

36. Revollo L, Kading J, Jeong SY, Li J, Salazar V, Mbalaviele G, et al. N-cadherin restrains PTH activation of Lrp6/beta-catenin signaling and osteoanabolic action. J Bone Miner Res. 2 2015;30(2):274–85. [PubMed: 25088803]

Highlights

1. Zfp467 −/− mice have increased bone mass and reduced adipose tissue.
2. Zfp467 −/− mice have higher level of Pth1r in bone and related cells.
3. Zfp467 −/− mice are resistant to OVX induced adiposity.
4. Zfp467 −/− mice are resistant to high fat diet-induced adiposity and weight gain.

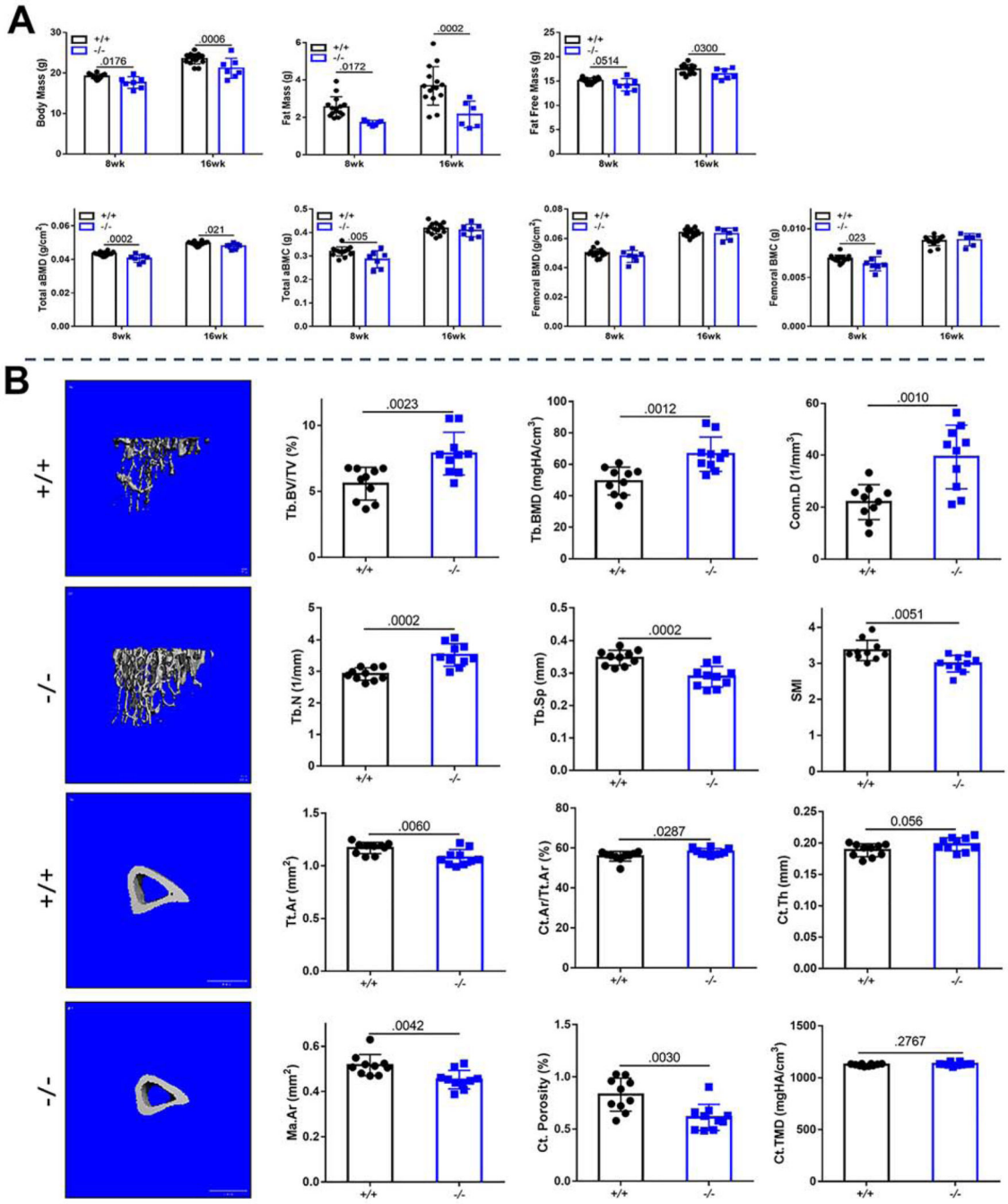

Fig. 1. *Zfp467*−/− are smaller and have higher trabecular and cortical bone mass.

16 weeks old +/+ and −/− mice were weighted and screened using Lunar PIXImus Densitometer for body composition including (A) body mass, fat mass, and fat free mass, total and femoral areal bone mineral density (fBMD, aBMD), femoral areal bone mineral content (fBMC, aBMC); (B) Representative μCt images of tibia trabecular and cortical bone of 16 weeks old +/+ and −/−. Trabecular microarchitecture was measured by μCT and trabecular bone volume/total volume (Tb.BV/TV), trabecular bone mineral density (Tb.BMD), connectivity density (Conn.D), trabecular number (Tb.N), trabecular separation

(Tb.Sp), and structural modeling index (SMI) were calculated. Total area (Tt.Ar), cortical area/total area (Ct.Ar/Tt.Ar), cortical thickness (Ct.Th), marrow area (Ma.Ar), cortical porosity (Ct. Porosity), and cortical tissue mineral density (Ct.TMD) were also assessed. Data shown as mean ± SD, n=7–15 per group.

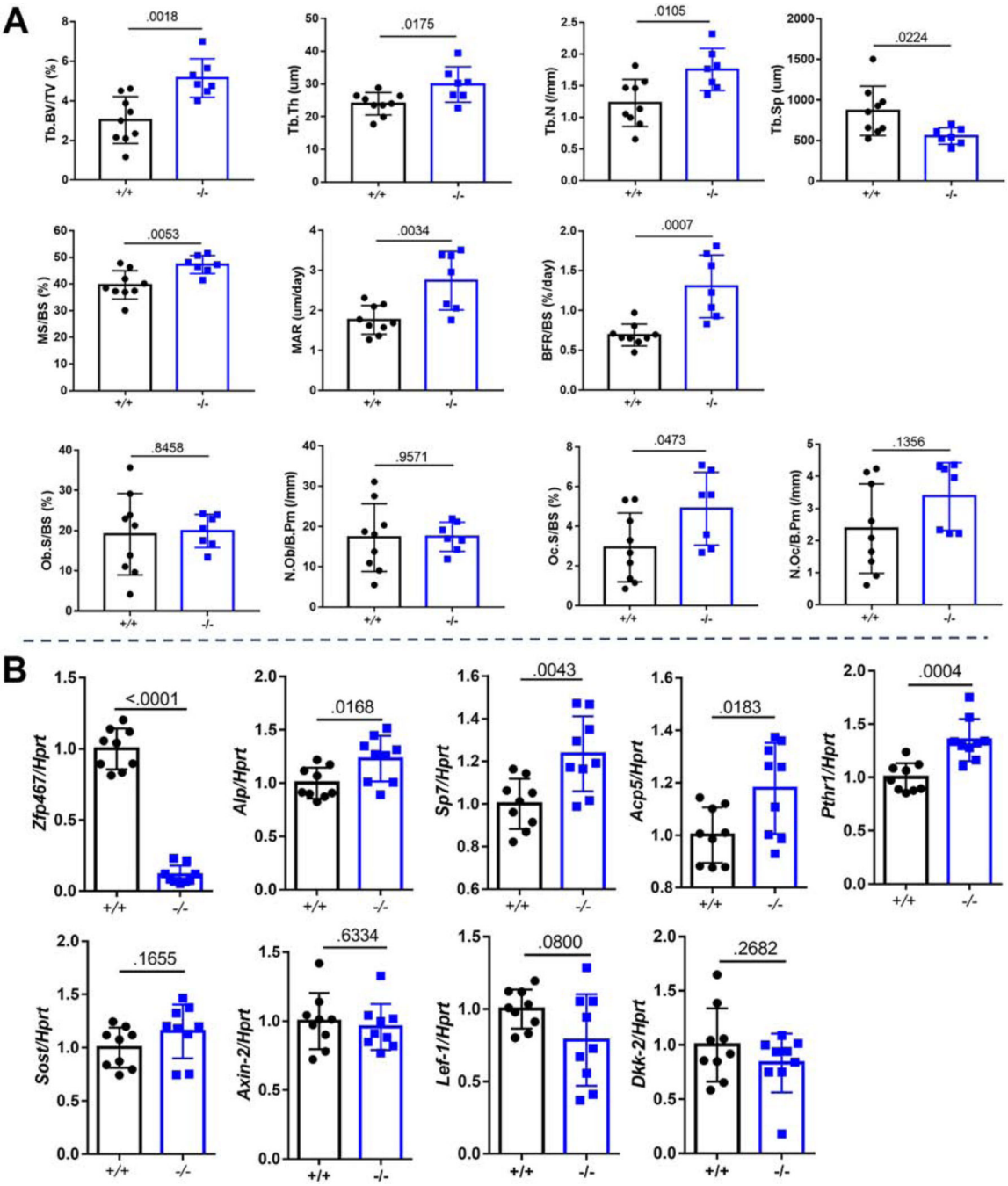

Fig. 2. *Zfp467*−/− mice have increased trabecular bone mass, bone formation, and osteoblast genes expression.

(A) Trabecular and cortical bones were assessed by static and dynamic histomorphometry in the tibia at 16wks of age. Tb = trabecular; BV/TV = bone volume/total volume; Th = thickness; N = number; Sp = separation; MS/BS = mineral surface/bone surface; MAR = mineral apposition rate; BFR/BS = bone formation rate/bone surface; Ob.S/B.Pm = osteoblast surface/bone perimeter; N.Ob/B.Pm = number of osteoblast/bone perimeter; Oc.S/B.Pm = osteoclast surface/bone perimeter; N.Oc/B.Pm = number of osteoclast/bone

perimeter; (B) Gene expression of whole femurs was analyzed by qRT-PCR in 16 weeks old mice. Data shown as mean ± SD, n=7–9 per group.

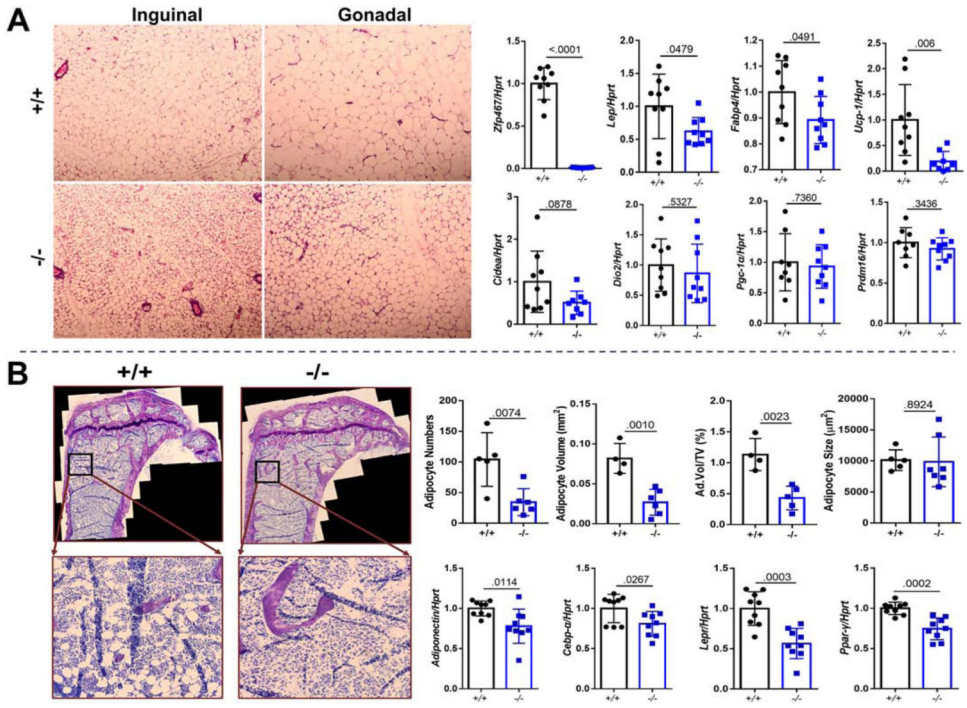

Fig. 3. *Zfp467*−/− mice have reduced peripheral and marrow adipose tissue.

(A) Inguinal and gonadal fat pads of 16 weeks old mice were isolated, paraffin embedded, and stained with H&E. Representative images of inguinal and gonadal fat pads at 10X. *Zfp467* −/− mice showed smaller adipocytes. qRT-PCR of adipogenesis related genes such as *Lep* and *Fabp4* were down regulated. *Ucp-1* was also found lower in −/− inguinal fat tissues, and other genes related to development of brown adipocytes such as *Cidea, DiO2, Pgc1a, and Prdm16* showed no remarkable difference between genotypes in inguinal fat of 16 weeks old mice. (B) Tibiae of 16 weeks old mice were processed, plastic embedded, stained with toluidine blue, and quantified for marrow adipocytes using a BIOQUANT OSTEO software. *Zfp467*−/− mice have lower marrow adipocyte number, adipocyte volume, and adipocyte volume/tissue volume vs. +/+ mice. Gene expression levels of *Adiponectin*, *Cebpa, Lepr,* and *Pparγ* in femurs of 16 weeks old mice are significantly lower in −/−. Data shown as mean ± SD, n=5–9 per group.

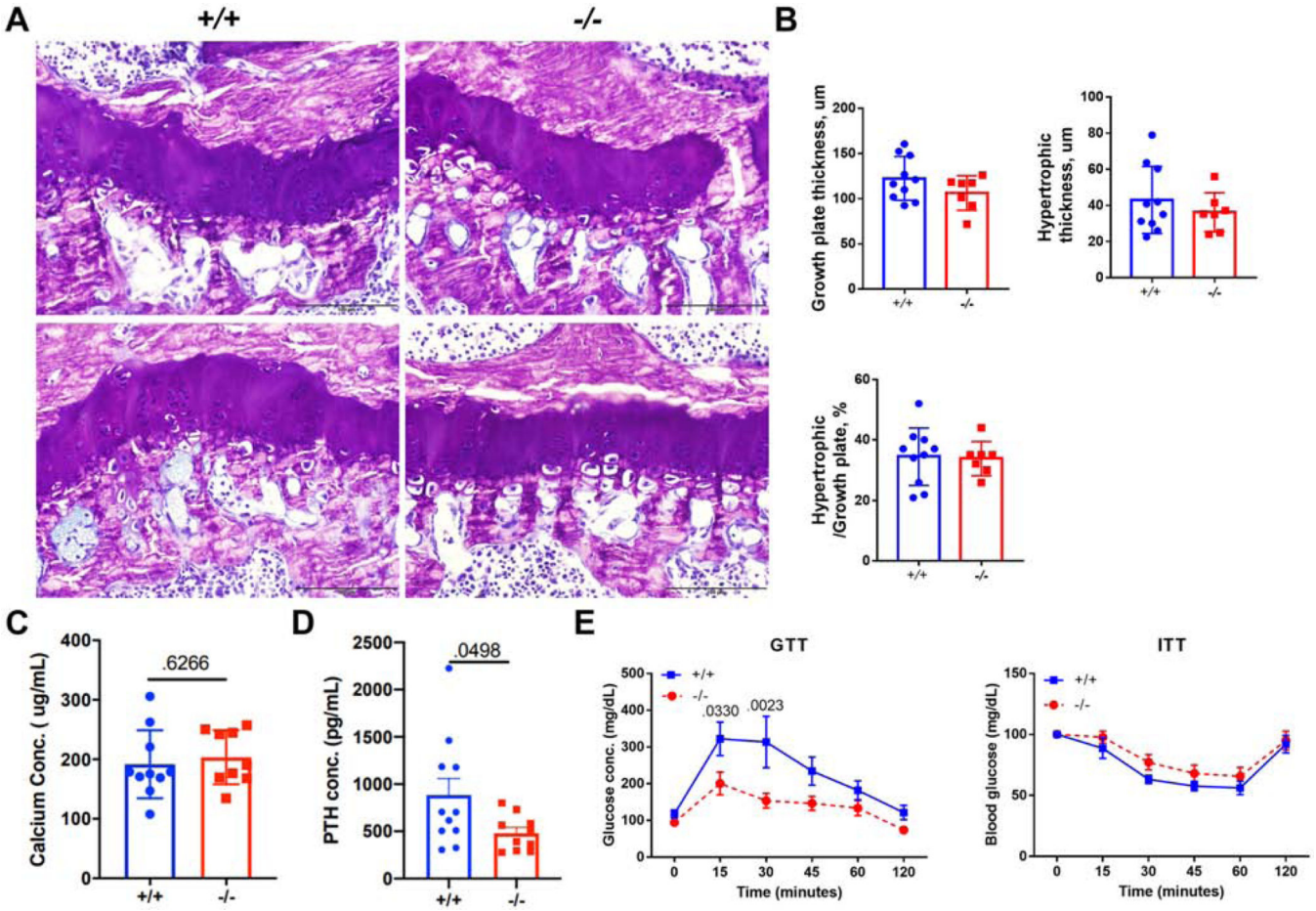

Fig. 4. Insulin and glucose tolerance tests.

Zfp467−/− mice at 15 weeks of age have improved glucose tolerance but no differences in insulin tolerance vs. +/+ mice. Data shown as mean ± SD, n=6–7 per group.

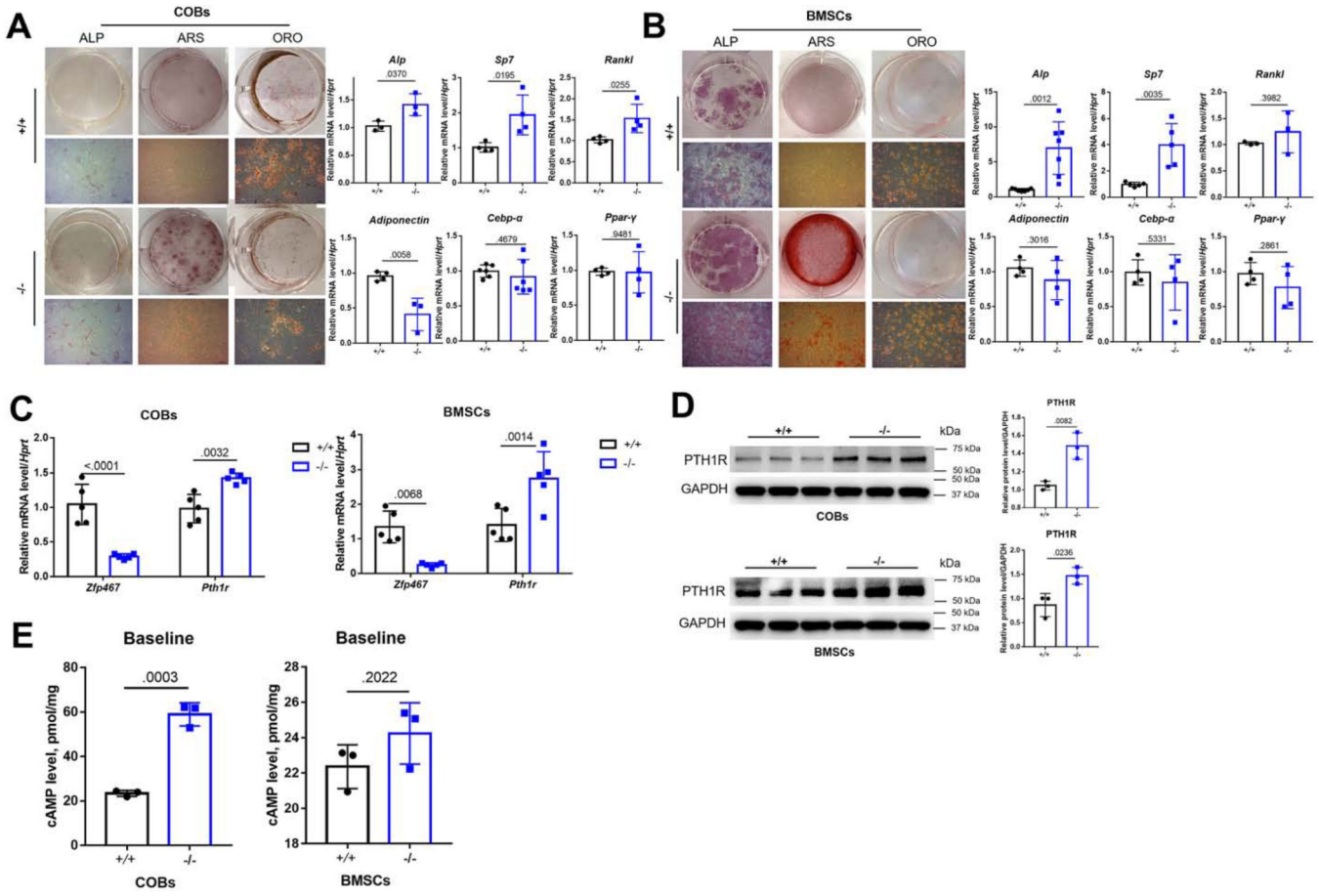

Fig. 5. *Zfp467*−/− show increased osteogenesis and decreased adipogenesis.

(A, B) Representative images of ALP (5X), Alizarin Red (5X), and Oil Red O (10X) stainings of COBs and BMSCs showing an increase in osteogenesis and decrease in adipogenesis in COBs. Gene expression of osteoblast and adiogenesis markers were analyzed by qRT-PCR in osteoblast and adipocyte differentiated cells; (C) qRT-PCR results of baseline COBs and BMSCs. Higher expression levels of *Pth1r* were found in both −/− COBs and BMSCs; (D) Western blot analysis of baseline COBs and BMSCs. Higher expression levels of PTH1R were found in both −/− COBs and BMSCs; (E) Cyclin adenosine monophosphate (cAMP) ELISA of COBs and BMSCs, −/− COBs cells displayed 3-fold higher cAMP compared to +/+ but no difference was found in BMSCs +/+ and −/−; (F) PTH treatments significantly suppressed *Zfp467* expression within 10 minutes of treatment in both +/+ COBs and BMSCs. Data shown as mean ± SD, n=3–6 per group.

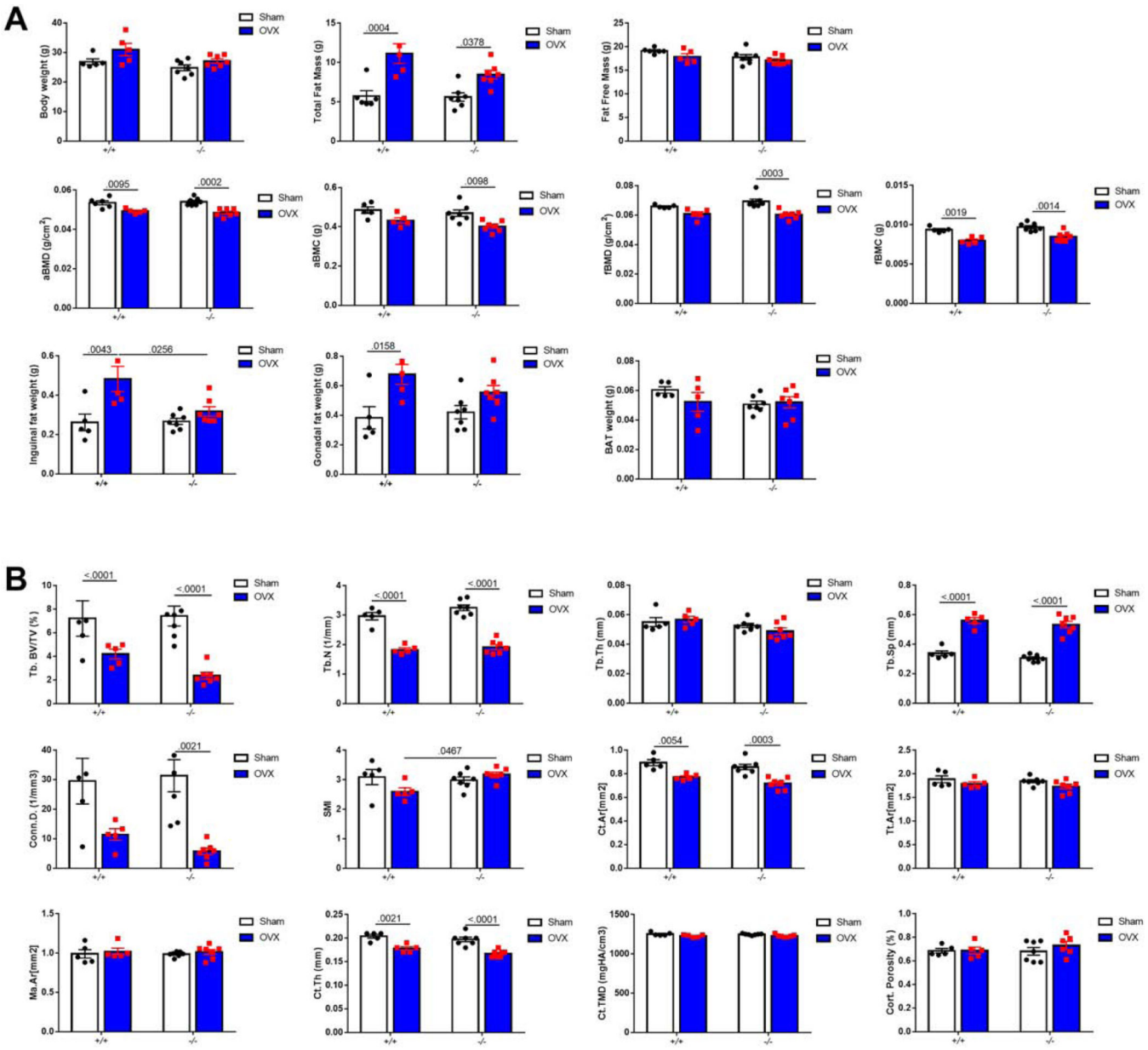

Fig. 6. *Zfp467*−/− had better resistance to high fat diet induced adipocytes accumulation and higher bone formation.

16 weeks old female +/+ and −/− mice fed with LFD or HFD were weighted (body weight, inguinal fat weight, gonadal fat weight and brown fat weight) and screened using Lunar PIXImus Densitometer for body composition including (A) body mass, fat mass, and fat free mass, total and femoral areal bone mineral density (fBMD, aBMD), femoral areal bone mineral content (fBMC, aBMC); (B) Representative μCt images of tibia trabecular and cortical bone of 16 weeks old female +/+ and −/− mice fed with LFD or HFD. Trabecular microarchitecture was measured by μCT and trabecular bone volume/total volume (Tb.BV/TV), trabecular bone mineral density (Tb.BMD), connectivity density (Conn.D), trabecular number (Tb.N), trabecular separation (Tb.Sp), and structural modeling index (SMI) were calculated. Total area (Tt.Ar), cortical area/total area (Ct.Ar/Tt.Ar), cortical thickness

(Ct.Th), marrow area (Ma.Ar), cortical porosity (Ct. Porosity), and cortical tissue mineral density (Ct.TMD) were also assessed. Data shown as mean ± SD, n=4–8 per group.

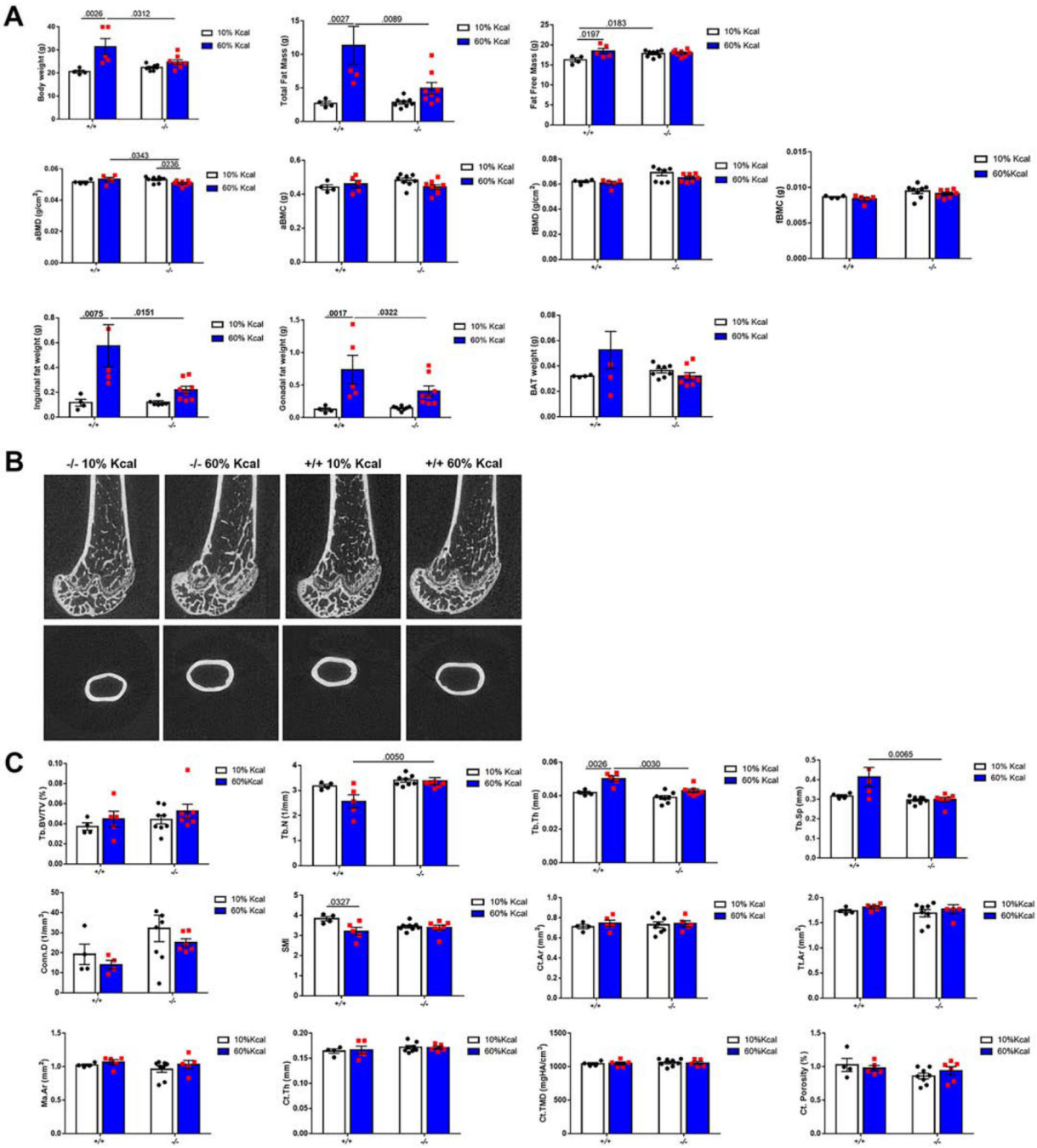

Fig. 7. *Zfp467*−/− showed better resistance to OVX induced adipocytes accumulation but not bone loss

16 weeks old female +/+ and −/− mice with OVX or sham surgery were weighted (body weight, inguinal fat weight, gonadal fat weight and brown fat weight) and screened using Lunar PIXImus Densitometer for body composition including (A) body mass, fat mass, and fat free mass, total and femoral areal bone mineral density (fBMD, aBMD), femoral areal bone mineral content (fBMC, aBMC); (B) Representative μCt images of tibia trabecular and cortical bone of 16 weeks old female +/+ and −/− mice fed with OVX or sham surgery. Trabecular microarchitecture was measured by μCT and trabecular bone volume/total

volume (Tb.BV/TV), trabecular bone mineral density (Tb.BMD), connectivity density (Conn.D), trabecular number (Tb.N), trabecular separation (Tb.Sp), and structural modeling index (SMI) were calculated. Total area (Tt.Ar), cortical area/total area (Ct.Ar/Tt.Ar), cortical thickness (Ct.Th), marrow area (Ma.Ar), cortical porosity (Ct. Porosity), and cortical tissue mineral density (Ct.TMD) were also assessed. Data shown as mean ± SD, n=5–7 per group.

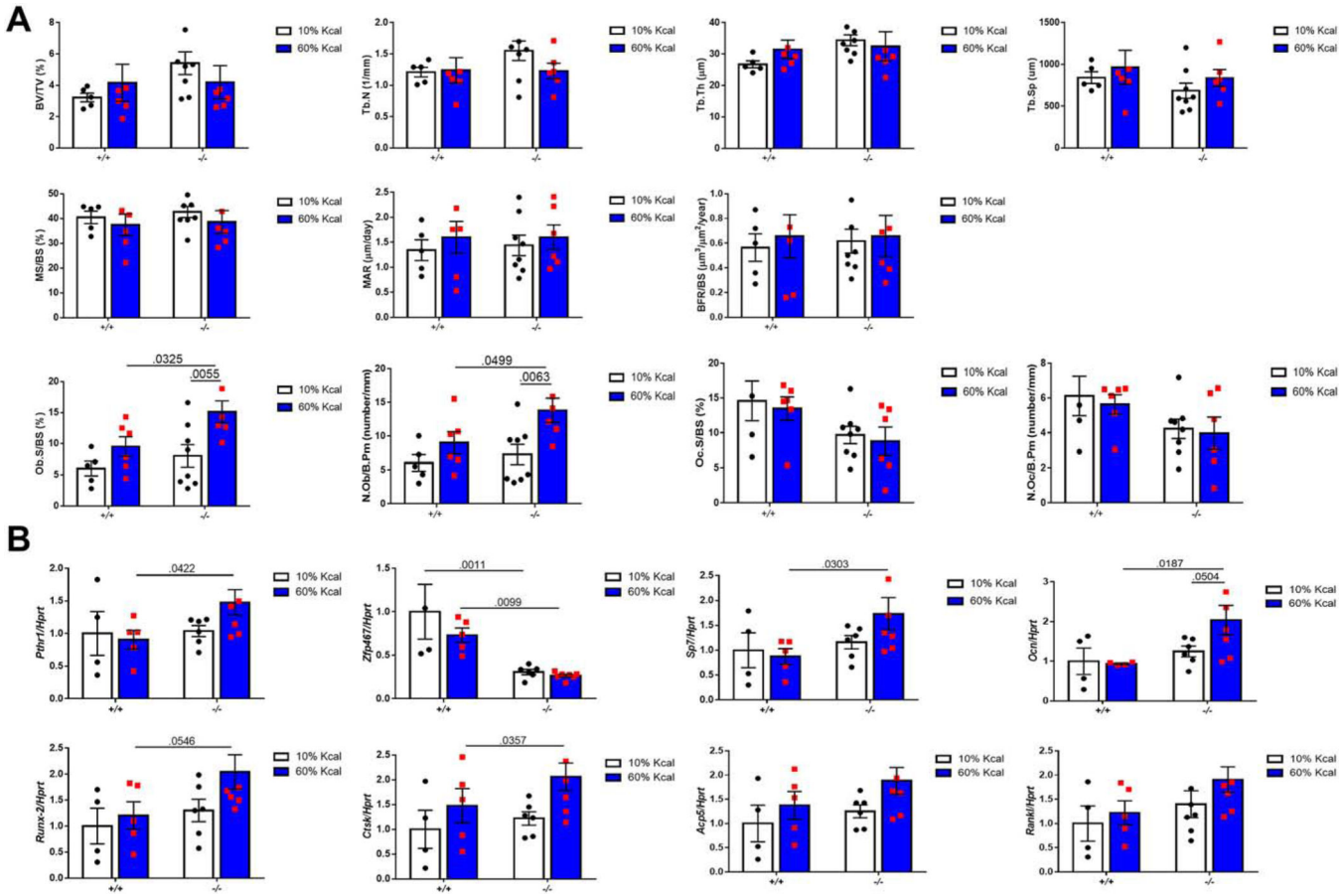

Fig. 8. *Zfp467*−/− mice have increased osteoblasts, and osteoblast genes expression with HFD.

(A) Trabecular and cortical bones were assessed by static and dynamic histomorphometry in the tibia at 16wks of age. Tb = trabecular; BV/TV = bone volume/total volume; Th = thickness; N = number; Sp = separation; MS/BS = mineral surface/bone surface; MAR = mineral apposition rate; BFR/BS = bone formation rate/bone surface; Ob.S/B.Pm = osteoblast surface/bone perimeter; N.Ob/B.Pm = number of osteoblast/bone perimeter; Oc.S/B.Pm = osteoclast surface/bone perimeter; N.Oc/B.Pm = number of osteoclast/bone perimeter; (B) Gene expression of whole femurs was analyzed by qRT-PCR in 16 weeks old mice. Data shown as mean ± SD, n=5–7 per group.

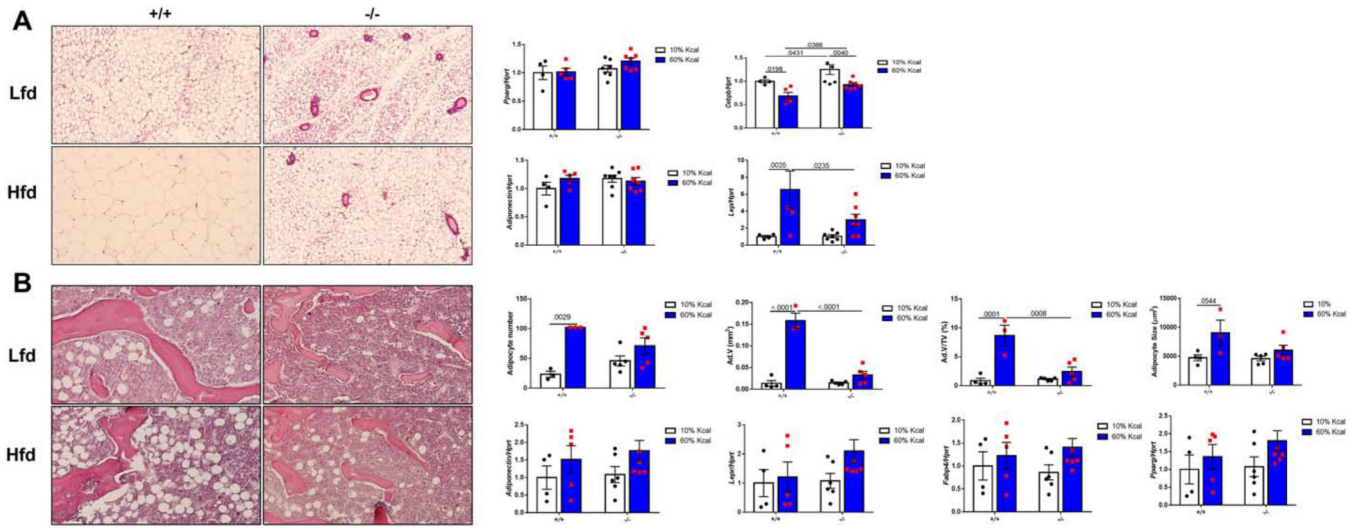

Fig. 9. *Zfp467*−/− had limited peripheral and marrow adipose tissue increasing with HFD vs. *Zfp467*+/+.

(A) Inguinal fat pads of 16 weeks old mice with LFD or HFD were isolated, paraffin embedded, and stained with H&E. Representative images of inguinal fat pads at 10X. qRT-PCR of adipogenesis related genes such as *Pparg, Cebpa, Adiponectin* and *Leptin* were analyzed in inguinal fat of 16 weeks old mice; (B) Tibiae of 16 weeks old mice were processed, plastic embedded, stained witt H&E, and quantified for marrow adipocytes using a BIOQUANT OSTEO software. Gene expression levels of *Adiponectin*, *Cebpa, Lepr, Fabp4* and *Pparγ* in femurs of 16 weeks old mice were analyzed. Data shown as mean ± SD, n=3–7 per group.